I&EC research
Industrial & Engineering Chemistry Research

pubs.acs.org/IECR

Article

Membrane Adsorbers with Copolymer Coatings for the Separation of Actinides from Lanthanides (UO_2^{2+} and La^{3+})

Published as part of Industrial & Engineering Chemistry Research special issue "Inverse Design of Materials and Processes for Separations".

Priyanka Suresh, Lianna Johnson, and Christine E. Duval*

Cite This: *Ind. Eng. Chem. Res.* 2024, 63, 20373−20382

Read Online

ACCESS | Metrics & More | Article Recommendations | Supporting Information

ABSTRACT: Separating lanthanides from actinides is a common task in rare earth element mining and processing, medical isotope purification, nuclear forensics, and radioanalytical chemistry. Membrane adsorbers are emerging as a promising platform to perform such adsorptive separations. In this work, functional membrane adsorbers are synthesized by coating poly(ether sulfone) microfiltration membranes with polymeric ligands that contain ethylene glycol methacrylate phosphate (EGMP) as the ion-coordinating moiety. The composition of the polymeric ligands is controlled by copolymerizing EGMP with butyl methacrylate (BuMA) and 2-hydroxy ethyl methacrylate (HEMA). Equilibrium and time-resolved adsorption data were modeled to understand the thermodynamics and kinetics of complexation of UO_2^{2+} at pH 1 and pH 4. The data are compared to previously reported data for La^{3+} and the feasibility of on-column separation of UO_2^{2+} over La^{3+} is assessed by transport modeling in MATLAB. All synthesized membranes are selective for UO_2^{2+} over La^{3+}. At pH 1, the separation is improved with the presence of a nonbinding comonomer. At pH 4, the separation is worsened by the presence of a nonbinding comonomer.

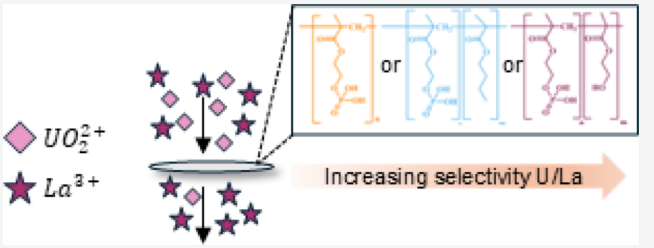

1. INTRODUCTION

The *f*-elements (lanthanides and actinides) have wide-ranging applications due to their unique fluorescent, magnetic, radioactive, and luminescent properties. The lanthanides constitute the majority of the rare earth elements that are used in modern technology such as clean energy generation, smartphones, and electric vehicles. Emerging sources of lanthanides include electronics recycling and recovery from actinide-containing phosphogypsum—a waste byproduct of phosphoric acid production in the fertilizer industry, which is produced at a rate of five tons per ton of phosphoric acid produced.[1] Currently, lanthanides are sourced through terrestrial mining and then separated using solvent extraction, which has several drawbacks. Not only does solvent extraction have a large physical footprint, but it also produces mixed organic radioactive waste and generates an average of 65.4 kg CO_2 per kg of lanthanide. In both mining and recovery from phosphogypsum—the separation of lanthanides from actinides is a crucial processing step. Therefore, improving the separation processes of actinides from lanthanides can have a key contributor to sustainability in the process of obtaining rare earth elements.

Organophosphorus ligands are widely used in the separation of actinides and actinides. For example, the PUREX process uses TBP (a neutral phosphate) and the TRansUranic EXtraction (TRUEX) process uses carbamoylmethylphosphine oxide (CMPO: a neutral phosphate).[2] The affinity of an organophosphorus ligand toward a particular actinide depends on the ligand chemistry and properties like charge, hydrophilicity, and formation of intramolecular H-bonds.[3] The "hardness", or propensity to form strong bonds with charge dense ions, of the P═O and thus its affinity for hard ions can be modulated by changing the chemical structure (i.e., local chemical environment) of the Lewis Base. For example, by elongating the alkyl chain (from n = 1 to n = 2, 3), Peters et al.[4] found that the distribution coefficients (K_d) of calixarene−CMPO derivatives toward Am^{3+} and Eu^{3+} both reduced by 2−3 orders of magnitude, under the same testing conditions. Vivero-Escoto et al.[5] functionalized commercially available mesoporous silica with a range of amidoxime, imide-dioxide, phosphonate, and carboxylic groups and investigated uranyl adsorption from pH 8 water and artificial seawater. They synthesized 4 adsorbents containing methyl phosphonate

Received: September 3, 2024
Revised: October 26, 2024
Accepted: October 29, 2024
Published: November 6, 2024

https://doi.org/10.1021/acs.iecr.4c03288
Ind. Eng. Chem. Res. 2024, 63, 20373−20382

groups: (1) methyl phosphonate, $PO(OH)(CH_3)$; (2) diethoxy-protected phosphonate, $PO(OC_2H_5)_2$; (3) deprotected mono phosphonate, $PO(OH)_2$; and (4) deprotected bisphononate $(PO(OH_2))_2$. Among the four phosphonate-modified silicas, the deprotected mono phosphonate-functionalized silica had the highest uranyl affinity. Wei et al.[6] synthesized phosphonate functionalized mesoporous silica through a "click" reaction of an azido group with phosphonate ligand. They controlled the overall surface charge of the adsorbent by introducing a positive charge through quaternizing unreacted azido groups. The K_d for UO_2^{2+}on the positive adsorbent at pH 7 was 2 orders of magnitude higher than the K_d for common competing ions in seawater (K^+, Ni^{2+}, Cu^{2+}, Zn^{2+}, and Pb^{2+}). The higher K_d for uranyl was attributed to its speciation at pH 7 where the anionic complex $[UO_2(CO_3)_3]^{4-}$ is dominant and experiences a strong Coulombic interaction with the positive ligand.

Alexandratos and Zhu[7] functionalized styrene resins with monoprotic phosphonic, diprotic phosphonic, and phosphonate ligands and evaluated the adsorption of UO_2^{2+}, and trivalent ions like Lu^{3+}, La^{3+}, Al^{3+}, and Fe^{3+} in 0.1−6 M phosphoric acid solutions. They found that the monoprotic ligand had the highest ion capacities due to the limited H-bonding between P═O and P−OH moieties. Inter- and intramolecular H-bonding reduces the electron density around the P═O. For monoprotic ligands, placing electronegative groups like oxygen in close proximity to P═O increases the overall ligand-ion affinity by providing additional sites for chelation. The same research group explored the effect of inter- and intramolecular H-bonding of polymer-supported organophosphorus ligands on the adsorption of trivalent and divalent ions,[8] divalent transition metals,[9] and UO_2^{2+}.[10] Through these works, they demonstrated that ligand affinity for UO_2^{2+} is impacted by (1) intra- and interligand H-bonding and (2) the presence of auxiliary functional groups near the primary coordination site on small molecule ligands.

While altering the ligand chemistry is a viable route to tune adsorption performance (affinity and capacity), designing new small molecules requires tedious synthetic organic chemistry efforts. To avoid such synthetic efforts, researchers have taken creative approaches to tune the local chemical environment of the complexing ligand by strategically placing different ligand chemistries near each other. In one embodiment of this concept Veliscek-Carolan et al.,[11] functionalized TiO_2 nanoparticles with tributyl phosphate, 1-amino-10-undecene, and a primary amine. Ligands were installed in a monolayer on the nanoparticle surface. Next, the TBP functional groups were spaced by diluting TBP with decene (1:10) during functionalization. Performance was evaluated using the extraction percentage of UO_2^{2+} from nitric acid solutions with pH 2−7. Interestingly, at pH 3 there was no difference in UO_2^{2+} extraction (%) between TBP-functionalized and TBP/decene-functionalized TiO_2 nanoparticles, despite a lower number of TBP moieties per nanoparticle. They attributed this to the conformational freedom of the spaced-out TBP functional groups; however, the authors were not able to quantify the performance enhancement since they did not estimate the number of functional groups. In a separate work, Alexandratos et al.[12] synthesized amidoxime (AO)-containing polyacrylonitrile fibers and functionalized the fibers with diethylenetriamine (DETA) or phosphorylated-DETA. Uranyl adsorption was evaluated in artificial and natural seawater. The fiber capacity for uranyl increased in the order AO > AO−DETA > AO−phosphorylated-DETA. Through FTIR analysis, they found that DETA interacts with AO through H-bonding which dissociates N−OH of the AO, thereby enhancing its affinity. The authors were unable to conclude whether DETA was directly complexing UO_2^{2+} ions using FTIR. The further enhancement of AO-phosphorylated-DETA was attributed to the secondary complexing sites provided by the phosphorylated-DETA. Finally, Chappa et al.[13] synthesized copolymer gels of ethylene glycol methacrylate phosphate (EGMP) with methyl methacrylate (MMA) or *N*-isopropylacrylamide (NIPA). The UO_2^{2+} extraction (%) from 0 to 5 $MHNO_3$ solutions was evaluated using an initial UO_2^{2+}concentration of 0.32 ppm. EGMP is an amphoteric ligand with a pK_{a1}= 1.60 and pK_{a2} = 6.62 thus the ligand is fully pronated at the tested conditions.[14] The extraction of UO_2^{2+} and Pu^{4+} by poly(EGMP) are similar, >80%. However, diluting the EGMP functional groups using MMA (1:10 ratio) greatly impacted the material's selectivity. For poly(EGMP-*co*-MMA), the UO_2^{2+} extraction (%) was near zero, while Pu^{4+} extraction remained high, >80%. Hence, changing the affinity of adsorbents for actinides is achievable by copolymerizing ligand-bearing monomers with diluting or "spacer" monomers. In all these embodiments, the underlying phenomena that drive the difference in affinity are complex and likely a combination of multiple factors like H-bonding, hydrophilicity, and charge density.

Radiochemists rely heavily on extractive and ion-exchange adsorbents for bench-scale radiochemistry separations. Recently, membrane adsorbers have emerged as a promising sample preparation platform for isotopic analysis of uranium and plutonium using alpha spectroscopy,[15−18] and an alternative to resin-packed columns for medical isotope purification.[19] The speed of the purification is particularly important for these applications since nuclear forensics and the purification of short-lived radiopharmaceuticals have strict timelines. To date, actinide-complexing ligand chemistries installed on membrane adsorbers have mirrored other actinide adsorbents, including phosphonic acids, phosphates, and amidoximes; however, there is some variation in the techniques used to impart membrane functionality. Foster et al.[17] prepared Pu-extractive thin film composite membranes by spin coating poly(4-methylstyrene-*co*-EGMP) on ultrafiltration membranes. The thin film composite membranes were used to extract trace levels (4−5 Bq mL^{-1}) of Pu-242 from pH 4 and 6 nitric acid solutions. Membrane permeance was high 63.1 L m^{-2} h^{-1} bar^{-1} (LMH bar^{-1}) and Pu-242 recovery during filtration was ∼10% at a transmembrane pressure of 0.69 bar. In a related work, Foster et al.[16] fabricated Pu-extractive membranes from a blend of polyvinylidene fluoride (PVDF) and PVDF-graft-EGMP by a nonsolvent induced phase separation process. The resulting membranes had high permeance (up to 50 LMH bar^{-1} depending on casting conditions), while Pu-238 recovery was 60% from pH 6 water and 19% from pH 6.58 synthetic seawater when filtered at a transmembrane pressure of 0.69 bar. Darge et al.[18] took a different approach by chemically modifying commercial polyacrylonitrile ultrafiltration membranes (MWCO, 30−400 kDa) to impart an amidoxime surface chemistry for UO_2^{2+} capture from pH 4, 6, and 8 solutions. Though membrane permeance decreased after functionalization, it remained high, e.g., 80 LMH bar^{-1}. Breakthrough studies indicate that up to the maximum flow rate tested in the study, 2 mL min^{-1}, uranyl

https://doi.org/10.1021/acs.iecr.4c03288
Ind. Eng. Chem. Res. 2024, 63, 20373−20382

capture is limited by the amidoxime−uranyl complexation kinetics and not mass transport through the membrane.

In this work, we employ a UO_2^{2+} complexing membrane adsorber that consists of a commercial microfiltration membrane coated with functional polymers. The functional coating relies on EGMP as the UO_2^{2+} complexing ligand and is formed by thermal polymerization around the membrane support. Three functional polymer coatings are explored: (1) EGMP homopolymer; (2) EGMP copolymerized with 2-hydroxyethyl methacrylate (HEMA), an H-bond donor; and (3) EGMP copolymerized with butyl methacrylate (BuMA), an H-bond nonparticipant. We hypothesized that the selectivity of the EGMP-containing coatings would be altered by systematically introducing auxiliary comonomers into the EGMP-containing polymer chain. The adsorption capacity, affinity, and kinetics of the three functionalized membranes for UO_2^{2+}, a representative actinide, are evaluated at pH 1 and pH 4. These conditions represent two distinct ionization states of the EGMP monomer: fully protonated at pH 1 and singly protonated at pH 4. We draw comparisons from our recent work,[20] which investigated the complexation of the same three functional membranes with La^{3+}, a representative lanthanide, at the same conditions. This combined analysis provides practical insights into designing functional membrane adsorbers for selective lanthanide-actinide separations.

2. EXPERIMENTAL SECTION

2.1. Materials and Reagents. DI Water from the RiOS 3-DI 3 system (Millipore Sigma, Burlington, Massachusetts) was used for all experiments. Poly(ether sulfone) (PES) microfiltration membranes (0.45 μm pore diameter, 130−155 μm thickness) were obtained from Millipore Sigma. Phosphoric acid 2-hydroxyethyl methacrylate ester (EGMP, 90%), 2−2-azobis(2-methylpropionitrile) (AIBN, 98%), dimethyl sulfoxide-d_6 (d_6-DMSO, MagniSolv MilliporeSigma, deuteration degree min. 99.8%), 2-hydroxyethyl methacrylate (HEMA, ≥ 99% with ≤50 ppm monomethyl ether hydroquinone inhibitor), and lanthanum(III) nitrate hexahydrate (99.99% trace metal basis) were procured from Sigma-Aldrich. Ethanol (99.5%) and butyl methacrylate (BuMA, 99%, stabilized with 4-methoxyphenol) were obtained from Acros Organics. Denatured ethanol (90%) and nitric acid (15.8N, certified ACS Plus, Safe-Cote) were procured from Fisher Scientific. Ultima Gold AB scintillation cocktail was obtained from PerkinElmer (Waltham, Massachusetts). A 1000 ppm uranium standard in 2% HNO_3 (assurance grade) was obtained from SPEXCertiPrep (Metuchen, New Jersey). U-233 in the form of uranyl nitrate in 1 M HNO_3 (18 KBq, Calibrated and NIST traceable) was procured from Eckert and Ziegler (Atlanta, GA, USA).

2.2. Membrane Synthesis. Three membrane designs were used in this work: poly(EGMP)-, poly(EGMP-*co*-BuMA)-, and poly(EGMP-*co*-HEMA)-functionalized membranes. Membranes were synthesized by modifying commercial PES membranes by using thermally induced free radical polymerization. The detailed description of the membrane functionalization and characterization is explained in a companion paper.[20] For clarity, an overview of the process is described here. Briefly, monomers EGMP, BuMa, HEMA, or desired combinations thereof were dissolved in ethanol in a 1:1 molar ratio. The concentration of monomers was optimized using trial-and-error to gain a consistent mass of polymers across the different functionalized membranes. Thus, 4 mmol of EGMP was dissolved in 20 mL of ethanol to synthesize poly(EGMP)-functionalized membranes. Four mmol of each monomer was dissolved in 12 mL of ethanol to synthesize poly(EGMP-*co*-BuMA) and poly(EGMP-*co*-HEMA)-functionalized membranes. AIBN, the thermal free-radical initiator, was dissolved in the monomer solution (10 wt % of the monomer mass). After mixing, the initiator-containing monomer solution was pipetted onto a PES membrane inside a 50 mL glass jar (Fisherbrand) with a threaded lid. The membranes were swelled in the monomer solution for 15 min. Then jars were heated to 77 ± 2 °C, which is above the activation temperature of AIBN (10-h half-life at 65 °C) [27] and below the normal boiling point of ethanol (78 °C). After the reaction, membranes were rinsed with denatured ethanol, soaked overnight in denatured ethanol, and dried overnight at 100 °C under a 25 mmHg vacuum.

The resulting polymer structures are listed in Figure 1. Poly(EGMP) is a homopolymer of EGMP. Poly(EGMP-*co*-BuMA) and poly(EGMP-*co*-HEMA) are copolymers of EGMP with BuMA (hydrophobic, does not H-bond) and HEMA (hydrophilic, H-bond donor). In this work, the functional polymers are physically coated on the membrane surface and pores.

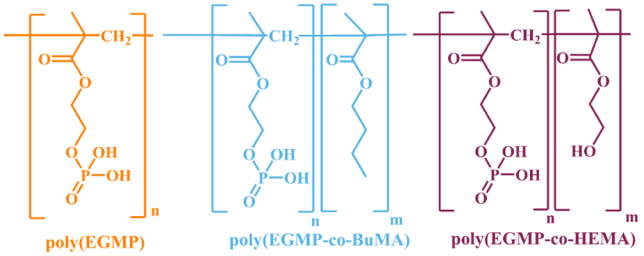

Figure 1. Chemical structures of the functional polymers coated on the PES microfiltration membranes: poly(EGMP), poly(EGMP-*co*-BuMA), and poly(EGMP-*co*-HEMA). EGMP is diprotic and engages in H-bonding. BuMA is a H-bond nonparticipant. HEMA is an H-bond donor.

2.3. Membrane Characterization. The characterization of these membranes was reported and discussed in detail in the companion paper[20] and an overview of the membrane properties relevant to this paper is given in Section 3.2. The membrane chemical composition before and after functionalization was observed using attenuated total reflectance Fourier transform infrared spectroscopy (ATR-FTIR) and nuclear magnetic resonance (^{1}H NMR) spectroscopy. The surface morphology of the membranes was imaged by using scanning electron microscopy (SEM). Water contact angle goniometry was performed to probe the surface hydrophilicity. Water uptake (%) measurements reflect the swelling of the membrane in water. Membrane permeance was measured by using dead-end filtration.

2.3.1. X-Ray Photoelectron Spectroscopy (XPS). To estimate the atomic ratio of U to P (an indicator of ligand sites), membranes were analyzed by using XPS before and after UO_2^{2+} adsorption. An XPS spectrum was collected for unmodified PES membranes to ensure all measured P was attributed to the EGMP ligand. Membranes were loaded with UO_2^{2+} by soaking one single membrane in a pH 1 or pH 4 solution of 100 ppm depleted UO_2^{2+} solution for 24 h. The uranyl solutions were prepared by diluting 1000 ppm of depleted uranium standard with DI water. The pH was

https://doi.org/10.1021/acs.iecr.4c03288
Ind. Eng. Chem. Res. 2024, 63, 20373−20382

adjusted using 16 M HNO_3 and/or 2 M NaOH as required. The final uranyl concentration was calculated after a pH adjustment. After soaking, membranes were removed from the solution and dried at 100 °C in a vacuum oven (P = 25 mmHg). Surface contaminants were removed from dried membrane samples by sputter cleaning with an Ar ion gun (2 kV, 2 mm × 2 mm at 2 μA) at a rate of 8.1 nm min^{-1} for 12 s. The XPS of sputter-cleaned samples were collected in a PHI 500 Versaprobe with a 200 μm monochromatized AI source (pass energy of 93.9 eV at a range of 0−1100 eV, energy step of 0.4 eV at 25 mS/step, and 11 scans).

2.4. Membrane Adsorption Performance. *2.4.1. Equilibrium Adsorption of UO_2^{2+}.* Equilibrium adsorption experiments were conducted using poly(EGMP), poly(EGMP-*co*-BuMA), poly(EGMP-*co*-HEMA) and UO_2^{2+} solutions at pH 1 and pH 4. Additionally, control experiments were conducted using unmodified PES, poly(BuMA)-functionalized, and poly(HEMA)-functionalized membranes to ensure that all UO_2^{2+} adsorption is attributed to the EGMP-containing polymers. All adsorption experiments were performed at pH 1 and pH 4. Uranyl solutions in the concentration range 1−100 ppm (1, 2, 5, 10, 25, 50, and 100 ppm) were prepared by serial dilutions of the 1000 ppm depleted uranium standard. The pH of the uranyl solutions was adjusted to pH 1 ± 0.1 using 16 M HNO_3 or pH 4 ± 0.1 using 4 M HNO_3 and/or 2 M NaOH as required. Each 100 mL of the diluted uranyl solutions was spiked with 0.85 mL of U-233 tracer (A = 32.6 mBq/mL). The U-233 tracer solution was diluted from an 18 kBq NIST-traceable U-233 liquid source.

Equilibrium adsorption experiments were performed by adding 15 ± 0.2 mg of membrane to 15 mL of UO_2^{2+} solution in 20 mL PET scintillation vials with lined threaded caps (Wheaton, DWK Life Sciences). The vials were mixed for 24 h on a shaker table (Labline Orbit Environ-shaker) at 150 rpm and ambient temperature. The initial and equilibrium concentrations of the uranyl solutions were measured using a Quantulus GCT Liquid Scintillation Counter (PerkinElmer Inc., Massachusetts). To prepare samples for liquid scintillation counting, 10 mL of each sample was mixed with 10 mL of Ultima Gold AB scintillation cocktail. The counting time for each sample was 1 h which was sufficient to achieve a minimum of 1000 counts in the region of interest. The instrument was calibrated using a 76.38 Bq U-233 standard prepared from the dilution of a NIST traceable U-233 liquid source to covert CPM to DPM. Background spectra were collected using 10 mL of pH 1 and pH 4 DI water. Reported error bars reflect the standard deviation of 3 different adsorption experiments using membranes modified by the same experimental procedures.

The uranyl adsorbed at equilibrium (Q_e, mmol UO_2^{2+} (g of membrane)$^{-1}$) was calculated according to eq 1.

$$Q_e = \frac{(C_0 - C_e)V}{m} \tag{1}$$

where, C_0 is the initial UO_2^{2+} concentration (mM), C_e is the equilibrium UO_2^{2+} concentration (mM), V is the volume of the UO_2^{2+} solution in the vial (L), and m is the mass of the membrane (g).

2.4.2. Time-Resolved Adsorption of UO_2^{2+}. Uranyl adsorption was monitored over time to understand how the kinetics of adsorption are impacted by the different functional coatings at pH 1 and pH 4. Kinetic experiments were performed by adding 5 ± 0.5 mg of membrane to a 15 mL solution of U-233 (36.9 Bq mL^{-1}) in a 20 mL borosilicate glass vial (Wheaton, DWK Life Sciences). Aliquots of 50 μL volume were drawn from the vial at 17 different time points between 5 min and 24 h. Aliquots were drawn more frequently in the first 3 h of the experiment to capture the characteristic shape of the adsorption curve.

The 50 μL aliquots were mixed with 10 mL of Ultima Gold AB scintillation cocktail for quantification using a Quantulus GCT Liquid Scintillation Counter (PerkinElmer Inc., Massachusetts). The counting time for each sample was 2 h, and a minimum of 100 counts was achieved for the initial solution in this counting period. Errors reported are standard errors from 3 different trials using membranes modified using the same experimental conditions.

The mass of UO_2^{2+} adsorbed at a given time t, Q_t (mmol UO_2^{2+}) (g of membrane)$^{-1}$ was calculated using eq 2.

$$Q_t = \frac{(C_0 - C_t)V}{m} \tag{2}$$

where C_0 is the initial concentration of UO_2^{2+} (mM), C_t is the concentration of UO_2^{2+} at time t (mM), V is the volume of the UO_2^{2+} solution (L), and m is the mass of the membrane (g).

The kinetic data were fitted with the pseudo-first order, pseudo-second order and Weber−Morris equations to identify the rate-determining step in the adsorption process.[21,22] The pseudo-first order model, given by eq 3, assumes that ion diffusion through the boundary layer is the rate-limiting step.

$$\ln\ln(Q_e - Q_t) = \ln\ln Q_e - k_1 t \tag{3}$$

Where k_1 (min^{-1}) is the rate constant of pseudo-first order adsorption, Q_e and Q_t (mg UO_2^{2+} g^{-1}) are the masses of UO_2^{2+} adsorbed at equilibrium and time t (min), respectively. The pseudo-second order model, given by eq 4, assumes that ligand−ion complexation is the rate-limiting step.

$$\frac{t}{Q_t} = \frac{1}{k_2 \cdot Q_e^2} + \frac{t}{Q_e} \tag{4}$$

Where k_2 (g membrane (mg UO_2^{2+} $min)^{-1}$) is the pseudo-second-order rate constant. The Weber−Morris model, given by eq 5, assumes that the intraparticle diffusion is the rate-limiting step.

$$Q_t = k_3 \cdot t^{0.5} + C \tag{5}$$

Where k_3 (mg UO_2^{2+} g membrane^{-1} $min^{-0.5}$) is the intraparticle diffusion rate constant and C (mg UO_2^{2+} g membrane^{-1}) is a constant proportional to the boundary layer. The value of C is directly proportional to the contribution of boundary layer diffusion step to the intraparticle diffusion.

2.5. Membrane Selectivity Calculated by Separation Factor. The distribution coefficient, K_d, is the ratio of the concentration of an ion adsorbed onto the solid adsorbent (membrane) to the ion concentration in the liquid phase. K_d is often used in the radiochemistry literature to report the adsorption performance of the adsorbent and is given by eq 6. While K_d is useful to compare the performance of an adsorbent for multiple ions, it is only valid for a given mass of the adsorbent at a given pH and concentration of the solution.

$$K_d = \frac{C_0 - C_e}{C_e}\left(\frac{V}{m}\right) \tag{6}$$

https://doi.org/10.1021/acs.iecr.4c03288
Ind. Eng. Chem. Res. 2024, 63, 20373−20382

Table 1. Summary of Key Membrane Properties for the Three Different Functionalized Membranes from Suresh et al[a 20]

Functionalized Membrane	Mass gain[b] (%)	Mass gain (mg polymer) (g membrane)$^{-1}$	P content[c] (mmol P) (g membrane)$^{-1}$	Water uptake[d] at pH 7 (%)	Contact angle[e] (deg)
poly(EGMP)	38.5 ± 9.7%	0.25 ± 0.01	0.61 ± 0.09	143.7 ± 12.6	60.5 ± 4.6°
poly(EGMP-*co*-BuMA)	30.8 ± 4.4%	0.27 ± 0.02	0.54 ± 0.05	88.7 ± 3.5	111.5 ± 2.8°
poly(EGMP-*co*-HEMA)	40.3 ± 5%	0.29 ± 0.02	0.33 ± 0.08	189.5 ± 8.8	36.2 ± 2.9°

[a]Reproduced from ref.[20] Copyright [2022] American Chemical Society. [b]Gravimetric mass gain(%) $= \frac{\text{mass of modified membrane} - \text{mass of unmodified membrane}}{\text{mass of modified membrane}} \times 100$. [c]Calculated from elemental analysis. [d]Measured using sessile-drop method. [e]Water uptake(%) $= \frac{(\text{membrane mass after soaking in DI water}) - (\text{dry membrane mass})}{\text{dry membrane mass}} \times 100$.

Where K_d is the distribution coefficient (L g^{-1}), C_0 is the initial UO_2^{2+} concentration (mmol), C_e is the equilibrium UO_2^{2+} concentration (mmol), V is the volume of the UO_2^{2+} solution in the vial (L), and m is the mass of the membrane (g).

For equilibrium-based separations (such as batch adsorption), the separation between two ions by a given adsorbent is quantified by the separation factor, α. The separation factor is the ratio of distribution coefficients for the two ions involved in the separation, eq 7. The two K_d values must be calculated for the same pH, ion concentration, and mass/volume ratio of the adsorbent and solution. The α values for the separation La^{3+} and UO_2^{2+} were calculated at pH 1 and 4 using calculated K_d values.

$$\alpha_{U/La} = \frac{K_{d,U}}{K_{d,La}} \tag{7}$$

Where $K_{d,U}$ and $K_{d,La}$ are the distribution coefficients of ions UO_2^{2+} and La^{3+}, respectively.

2.6. Converting Equilibrium Adsorption Data Modeled by the Langmuir Isotherm to K_d. The equilibrium adsorption data (Q_e and C_e) can be modeled with well-known adsorption isotherms, such as Langmuir or Freundlich. Choosing a model depends on the physicochemical properties of the adsorbent, adsorbate, and the adsorption mechanism. In this work, the functional ligand (EGMP) of the adsorbent and the adsorbate UO_2^{2+} have strong, specific interactions, thus the data are modeled with the Langmuir isotherm.[23] The Langmuir adsorption isotherm is given in eq 8.

$$Q_e = \frac{Q_m K_L C_e}{1 + K_L C_e} \tag{8}$$

Where Q_m (mmol of UO_2^{2+}) (g of membrane)$^{-1}$ is the maximum capacity for UO_2^{2+}, K_L (mM^{-1}) is the Langmuir association constant, and C_e (mM) is the equilibrium concentration of UO_2^{2+}. C_e and Q_e are measured experimentally, while Q_m and K_L are calculated through nonlinear curve fitting. The calculated Q_m and K_L are characteristic of the adsorbent, pH, and analyte. They are independent of the adsorbent mass and solution volume. Thus, using eqs 1 and 8, it is possible to predict the equilibrium conditions (C_e and Q_e) for different initial concentrations, adsorbent masses, or solution volumes. This is an important distinguishing factor between Q_e modeled by isotherms and the distribution coefficient, K_d shown in eq 6.

2.7. Dynamic Adsorption Model. The measured kinetic and thermodynamic properties of each membrane chemistry was modeled as a packed bed reactor or column. The mass balance for the adsorbing metal ion (UO_2^{2+} or La^{3+}) is represented by eq 9.

$$\frac{dC_M}{dt}(i) = -u\frac{dC_M}{dz}(i) - \rho_p\left(\frac{1-\varepsilon}{\varepsilon}\right)\frac{dQ_t}{dt}(i) \tag{9}$$

The change in ion concentration with respect to position in the membrane is represented in eq 10.

$$\frac{dC_M}{dz}(i) = \frac{[C_M(i+1) - C_M(i-1)]}{2dz} \tag{10}$$

Ion adsorption at a given time in terms of rate constant is described by eq 11.

$$\frac{dQ_t}{dt}(i) = k_{on}C_M(i)(Q_m - Q_t(i)) - k_{off}Q_t(i) \tag{11}$$

where C_M is the metal ion concentration exiting the membrane (mM), t is time (min), i is the step size for bed length, u is linear velocity (cm min^{-1}), z is membrane or column thickness (cm), ρ_p is the membrane density (g cm^{-3}), and ε is bed porosity, Q_t is the adsorbed ion concentration (mmol ion (mg of membrane)$^{-1}$), k_{on} is the modeled adsorption rate constant (L of solution (mmol of ion min)$^{-1}$), Q_m is the maximum concentration of ions that can be adsorbed (mmol ion (mg membrane)$^{-1}$), and k_{off} is the modeled desorption rate constant (min^{-1}). MATLAB (R2022b) Curve Fitter app and eq 12 were used to obtain k_{on} and k_{off} values from time-resolved adsorption data.

$$Q_t = Q_e\{1 - e^{[-(k_{on}C_{M,t} + k_{off})t]}\} \tag{12}$$

The metal ion balance was solved in MATLAB (R2022b), so C/C_0 could be plotted versus time, creating a breakthrough curve. In these simulations, column geometry (porosity and thickness) was held constant to focus on comparing the impact of ligand chemistry on the column breakthrough.

3. RESULTS

3.1. Membrane Characterization. The physical and chemical characterization of the membranes was completed in a companion paper.[20] Key properties are summarized in Table 1. While the percent mass gain is similar across all three functionalized membranes, the EGMP content varies, as shown by the P content in the elemental analysis.

3.2. Equilibrium Adsorption Studies. *3.2.1. Equilibrium Adsorption at pH 1 and pH 4.* Uranyl adsorption experiments were performed at pH 1 and 4 for all three functionalized membranes to evaluate the diprotic EGMP monomer at

https://doi.org/10.1021/acs.iecr.4c03288
Ind. Eng. Chem. Res. 2024, 63, 20373−20382

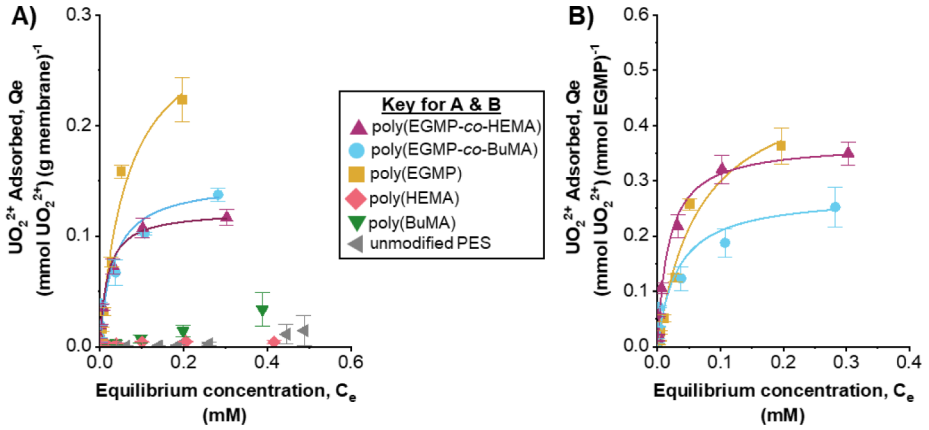

Figure 2. Equilibrium adsorption data for UO_2^{2+} at pH 1 on poly(EGMP)-, poly(EGMP-*co*-BuMA)-, and poly(EGMP-*co*-HEMA)-functionalized membranes. The adsorption data were modeled with a Langmuir adsorption isotherm on the (A) per membrane and (B) per mole of P basis.

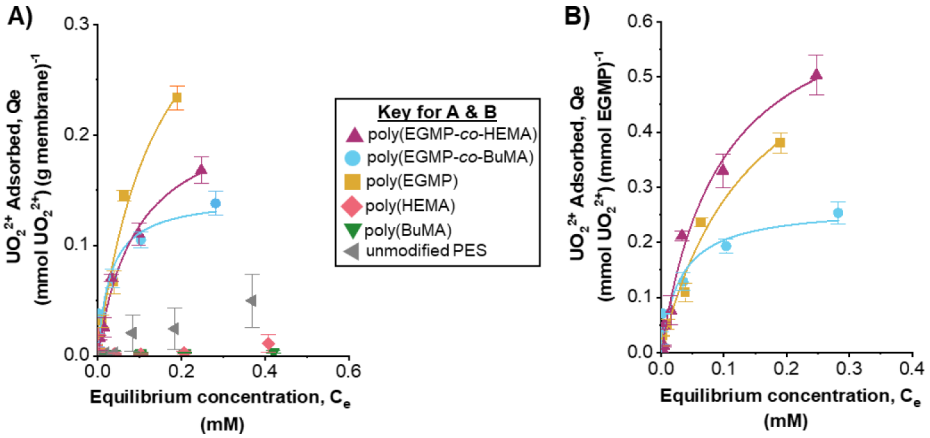

Figure 3. Equilibrium adsorption isotherms for UO_2^{2+} at pH 4 on membranes functionalized with poly(EGMP), poly(EGMP-*co*-BuMA), and poly(EGMP-*co*-HEMA). Adsorption data were modeled with the Langmuir adsorption isotherm. Control samples PES, poly(HEMA), and poly(BuMA) exhibit nonspecific adsorption. The adsorption is presented on (A) per membrane basis and (B) per moles of P basis.

Table 2. Langmuir Parameters (Q_m and K_L) for the Three EGMP-Containing Membranes at pH 1 and pH 4

pH	Functional Polymer	Maximum Capacity, Q_m mmol UO_2^{2+} (g membrane)$^{-1}$	Maximum Capacity, Q_m mmol UO_2^{2+} (mmol P)$^{-1}$	Langmuir Constant, K_L mM^{-1}	Stoichiometric Ratios at Q_m $UO_2^{2+}$to EGMP
1	poly(EGMP)	0.31 ± 0.03	0.50 ± 0.06	15.1 ± 4.0	1 to 2.0
1	poly(EGMP-*co*-BuMA)	0.15 ± 0.02	0.28 ± 0.04	31.8 ± 7.6	1 to 3.5
1	poly(EGMP-*co*-HEMA)	0.12 ± 0.01	0.37 ± 0.01	55.8 ± 8.7	1 to 2.8
4	poly(EGMP)	0.41 ± 0.07	0.67 ± 0.12	6.9 ± 2.3	1 to 1.5
4	poly(EGMP-*co*-BuMA)	0.14 ± 0.02	0.27 ± 0.04	33.0 ± 9.8	1 to 3.7
4	poly(EGMP-*co*-HEMA)	0.23 ± 0.02	0.69 ± 0.07	10.6 ± 2.4	1 to 1.5

different degrees of ionization (protonation). At pH 4, the EGMP is partially ionized (deprotonated) because it is in between pK_{a1} = 1.60 and pK_{a2} = 6.62 while at pH 1, it is fully protonated.[14] Adsorption data for UO_2^{2+} in pH 1 and pH 4 solutions are shown in Figures 2 and 3, respectively.

Importantly, the unmodified PES, poly(BuMA), and poly(HEMA) controls exhibit nonspecific adsorption across the range of concentrations tested. To account for the differences in P content, shown in Table 1, between the poly(EGMP), poly(EGMP-*co*-BuMA), and poly(EGMP-*co*-HEMA)-functionalized membranes, adsorption data were normalized to the moles of P. The adsorption curves for the EGMP-containing polymers at pH 1 and pH 4 are characteristic of strong adsorbate−adsorbent interactions and therefore were modeled with the Langmuir adsorption isotherm, eq 8. The model fitting parameters are reported in Table 2.

From the equilibrium adsorption data alone, it is challenging to draw conclusion about the differences in binding mechanisms across the three membranes and the two tested pH values; however, several trends can be identified by comparing the EGMP normalized data. Table 2 shows that at pH 1 the Q_m follows the trend: poly(EGMP) (0.50 ± 0.06 mmol UO_2^{2+} per mmol P) > poly(EGMP-*co*-HEMA) (0.37 ± 0.01 mmol UO_2^{2+} per mmol P) > poly(EGMP-*co*-BuMA) (0.28 ± 0.04 mmol UO_2^{2+} per mmol P). At pH 4, the Q_m follows the trend: poly(EGMP) (0.67 ± 0.12 mmol UO_2^{2+} per mmol P) = poly(EGMP-*co*-HEMA) (0.69 ± 0.07 mmol UO_2^{2+} per mmol P) > poly(EGMP-*co*-BuMA) (0.27 ± 0.04 mmol UO_2^{2+} per mmol P). Including a BuMA spacer has the same

https://doi.org/10.1021/acs.iecr.4c03288
Ind. Eng. Chem. Res. 2024, 63, 20373−20382

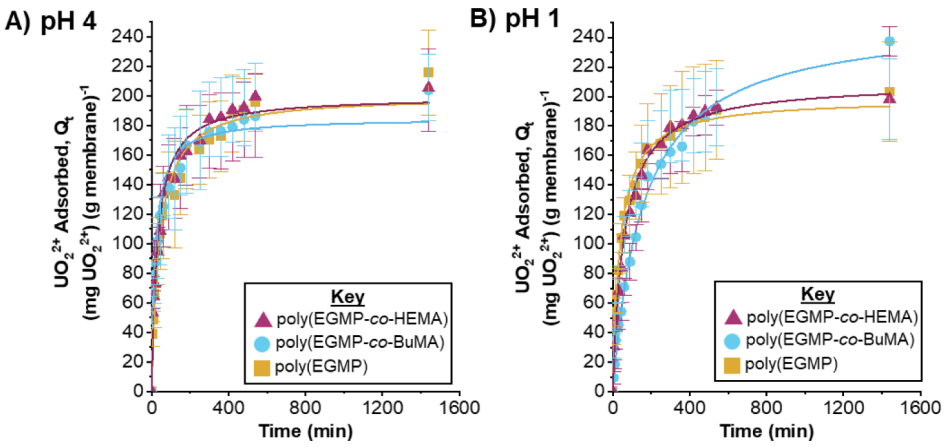

Figure 4. Adsorption of UO_2^{2+} over time at (A) pH 4 and (B) pH 1. The adsorption experiments were performed at 25 °C and follow pseudo-second order kinetics.

Table 3. Model Parameters (Equilibrium Capacity and Reaction Rate Constants) Obtained from a Pseudo-Second-Order Fit at pH 4 and 1 for UO_2^{2+} and La^{3+}[a]

		pH 4		pH 1		
		Equilibrium Capacity, Q_e	k_2	Equilibrium Capacity, Q_e	k_2	
Functional Polymer	Ion	μmol ion (g membrane)$^{-1}$	gmmol^{-1}min^{-1}	μmol ion (g membrane)$^{-1}$	g mmol^{-1}min^{-1}	Citation
poly(EGMP)	UO_2^{2+}	0.69 ± 0.03	37.7 ± 5.8	0.69 ± 0.03	37.7 ± 14.5	This work
poly(EGMP-*co*-BuMA)	UO_2^{2+}	0.66 ± 0.03	78.3 ± 14.5	0.86 ± 0.03	7.25 ± 0.67	This work
poly(EGMP-*co*-HEMA)	UO_2^{2+}	0.69 ± 0.03	46.4 ± 5.8	0.72 ± 0.03	23.5 ± 0.3	This work
poly(EGMP)	La^{3+}	9.36 ± 0.22	1.67 ± 0.14	11.0 ± 0.06	--	20
poly(EGMP-*co*-BuMA)	La^{3+}	9.94 ± 0.43	2.36 ± 0.42	10.8 ± 0.14	5.14 ± 0.42	20
poly(EGMP-*co*-HEMA)	La^{3+}	9.86 ± 0.29	0.83	11.1 ± 0.07	5.00 ± 0.42	20

[a]The lanthanum data was reproduced from ref.[20] Copyright [2022] American Chemical Society.

effect at pH 1 and 4 where the poly(EGMP-*co*-BUMA) capacity is nearly half of the poly (EGMP) capacity on a per EGMP basis. As shown in Table 1, the water uptake of poly(EGMP-*co*-BuMA) is 88.7 ± 3.5%, and the water uptake of poly(EGMP) is 143.7 ± 12.6%. One contributing factor may be that the poly(EGMP-*co*-BuMA) membranes swell less than the poly(EGMP) membranes in water and therefore some EGMP sites are inaccessible for complexation. This theory is consistent with the stochiometric ratios presented in Table 2. For BuMA-containing membranes, the ratios are 1 to 3.5 and 1 to 3.7 for pH 1 and 4, respectively; however, it is unclear if swelling alone can explain the 50% difference between the maximum capacities.

Interestingly, spacing the EGMP monomers with HEMA did not have the same effect on the capacity as spacing with BuMA at pH 4. As shown in Table 1, the contact angle of poly(EGMP-*co*-BuMA) is 111.5 ± 2.8° and the contact angle of poly(EGMP-*co*-HEMA) is 36.2 ± 2.9°. The hydrophilicity of poly(EGMP-*co*-HEMA) is further demonstrated by the high-water uptake of 189.5 ± 8.8%, whereas poly(EGMP-*co*-BuMA) was 88.7 ± 3.5%. In a related work,[13] introducing MMA monomers as spacers within an EGMP polymer reduced the adsorption (%) of UO_2^{2+}. Chappa et al. reasoned that the capacity was reduced in the presence of MMA because of UO_2^{2+} typical complexes with EGMP in a 1:2 ligand to ion ratio. Thus, by spacing the EGMP monomers, they suggested that there were fewer possible opportunities for UO_2^{2+} complexation. Furthermore, the hydrophobicity of the polymer gel inhibited swelling and a possible chain rearrangement to accommodate the 1:2 complexation motif. The higher swelling of the HEMA-containing system could increase the accessibility of the EGMP sites, resulting in a more complete utilization of the EGMP monomers for complexation. A second plausible phenomenon is that the hydroxyl (−OH) of the HEMA may stabilize the UO_2^{2+} complex with EGMP. Such a synergistic effect of comonomers in uranyl adsorption has been previously observed when the presence of pendant alcohols increased the affinity of phosphoric acid ligands for trivalent ions.[9] Finally, the hydroxyl of HEMA likely interacts with the phosphonic acid through H-bonding, which would impact the basicity of the phosphoryl oxygens. Without direct evidence of ligand-ion bond formation or computational modeling, it is not possible to deconvolute the possible contributions. From a practical standpoint, incorporating BuMA as a spacer monomer decreases the maximum capacity at pH 1 and 4 when compared to the poly(EGMP) homopolymer and the poly(EGMP-*co*-HEMA) copolymer.

At pH 4, the capacities of poly(EGMP-*co*-HEMA) and poly(EGMP) were statistically the same; however, at pH 1, the HEMA spacer appears to play a role different from that at pH 4. Without direct evidence of HEMA-UO_2^{2+} bond formation, a mechanistic conclusion cannot be definitively be drawn. At the very least, the practical implications of HEMA on membrane capacity are pH dependent.

The K_L (mM^{-1}) at pH 1 follow the trend: poly(EGMP-*co*-HEMA) (55.8 ± 8.7 mM^{-1}) > poly(EGMP-*co*-BuMA) (31.8 ± 7.6 mM_{-1}) > poly(EGMP) (15.1 ± 4.0 mM^{-1}). At pH 1 and 4, the poly(EGMP-*co*-BuMA)-functionalized membrane exhibit similar affinities while the poly(EGMP-*co*-HEMA)- and poly(EGMP)-functionalized membranes form stronger com-

https://doi.org/10.1021/acs.iecr.4c03288
Ind. Eng. Chem. Res. 2024, 63, 20373−20382

plexes at pH 1 than at pH 4. Another notable observation in the pH 4 equilibrium adsorption data is that the affinity (K_L) decreases with an increase in intermolecular H-bonding. The K_L values follow the order: poly(EGMP-*co*-BuMA) (33.2 ± 9.8 mM^{-1}) > poly(EGMP-*co*-HEMA) (10.6 ± 2.4 mM^{-1}) > poly(EGMP) (6.9 ± 2.3 mM^{-1}). Intermolecular H-bonding has been shown to reduces the basicity of the $p = O$[7,8] and in turn may reduce the EGMP affinity toward UO_2^{2+}. A similar effect was observed in our previous work with La^{3+} when using the same functionalized membranes.[20]

3.3. Time-Resolved Adsorption. The adsorption of UO_2^{2+} on the three functionalized membranes was measured over time at both pH 1 and pH 4 and modeled with eqs 3−5. The data was best modeled by the pseudo-second order equation—implying that the ligand-ion complexation reaction is the rate-limiting step. The kinetic curves are shown in Figure 4 and the model parameters from pseudo-second order are shown in Table 3. A representative set of data fitted with all the three equations is shown in Figure S1.

At pH 4, the reaction rate constants (k_2) follow the trend: poly(EGMP-*co*-BuMA) > poly(EGMP-*co*-HEMA) > poly-(EGMP). Practically, spacing the EGMP monomer with a BuMA increases the rate of complexation by a factor of 2 over poly(EGMP) or poly(EGMP-*co*-HEMA).

3.4. Comparison of Separation Performance. *3.4.1. Distribution Coefficients for Thermodynamic and Kinetic Separations.* The distribution coefficient, K_d, is commonly used to characterize the equilibrium performance of adsorbent materials for lanthanides and actinides. To situate this work within the literature, the K_d for each functionalized membrane was calculated and compared to other EGMP-functionalized solid adsorbents. As explained in Section 2.6, the K_d reported for an adsorbent material is valid only at the pH, adsorbate concentration, and mass-to-volume ratio used in its evaluation. By collecting the full isotherm, it is possible to predict the adsorbent performance at different starting concentrations and mass-to-volume ratios. In this way, the present work was compared to two relevant works in the literature.

Chappa et al.[13] synthesized poly(EGMP) gels for uranium sequestration and reported the K_d across a pH range −0.6 to 1. The adsorption experiments used a mass of 90 mg of sorbent, 10 mL of volume of solution, and an initial UO_2^{2+} concentration of 1.1 μM (0.32 ppm). Darge et al.[24] used spin coating to deposit a thin layer of poly(EGMP) on a silicon wafer while studying UO_2^{2+} adsorption in pursuit of an alpha spectroscopy substrate. The adsorption data was modeled with the Langmuir equilibrium isotherm and the Q_m and K_L were reported—enabling us to model the poly(EGMP) films at different conditions. The Q_m and K_L values for the present work and Darge's work were used in the Langmuir model to calculate a K_d at the same experimental conditions at the Chappa studies (as explained in Section 2.6). The reported and estimated K_d values were plotted as a function of pH in Figure 5.

Generally, the K_d of poly (EGMP) sorbents increases with increasing pH, Figure 5. Among the functionalized membranes in this study, the copolymer-functionalized membranes have marginally higher K_d for UO_2^{2+} than poly(EGMP), which is expected from the K_L.

At pH 4, the poly(EGMP) films reported by Darge et al.[24] show an order of magnitude higher K_d than the present work. In this work, the Q_m of the poly(EGMP) membranes is ∼2.9

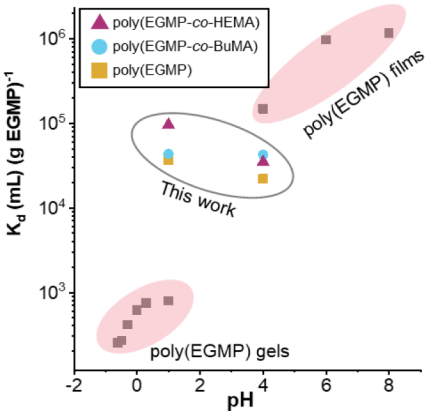

Figure 5. Distribution coefficients (K_d) for UO_2^{2+} on EGMP-functionalized materials reported in the literature[13,24] and the present work. Each K_d was calculated for an adsorbent mass of 90 mg of sorbent, 10 mL of solution, and an initial UO_2^{2+} concentration of 1.1 μM (0.32 ppm).

mmol of UO_2^{2+} (g of EGMP)$^{-1}$, which is significantly higher than the Darge poly(EGMP) films (∼0.3); however, at pH 4, the K_L of the poly(EGMP) films (439 mM^{-1}) is 2 orders of magnitude higher than this work's poly(EGMP) membranes (6.98 ± 2.34 mM^{-1}). Despite the same chemical functional groups, the physical form of the films appears to impact the adsorption—even when normalized to the moles of P.

3.4.2. Calculated Separation Factors Based on Equilibrium Data. As a first step toward evaluating the separation of lanthanides from actinides with these materials, the separation factor (α) was calculated according to eq 7. The K_d for each of the three functionalized membranes for La^{3+} and UO_2^{2+} were calculated using the data from the literature[20] and this work, Figure 6. Initial concentrations of La^{3+} and UO_2^{2+} were both 1.1 μM.

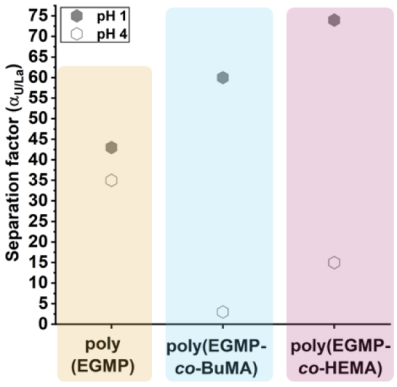

Figure 6. Separation factors $\alpha_{U/La}$ for poly(EGMP), poly(EGMP-*co*-BUMA), and poly(EGMP-*co*-HEMA) at pH 1 and pH 4. All membranes are selective for UO_2^{2+} over La^{3+} and show higher selectivity for UO_2^{2+} at pH 1 than at pH 4.

At pH 1, all $\alpha_{U/La}$ values are greater than 1 indicating a higher affinity for UO_2^{2+} compared to La^{3+}. Additionally, at pH 1, the addition of copolymers increases the separation between UO_2^{2+} and La^{3+} following the trend where poly(EGMP) = 43 < poly(EGMP-*co*-BUMA) = 60 < poly(EGMP-*co*-HEMA) = 74. On the other hand, at pH 4, the presence of BuMa or HEMA is detrimental to binding resulting in a lower K_d compared to poly(EGMP) where $\alpha_{U/La}$:poly(EGMP) = 35 >

https://doi.org/10.1021/acs.iecr.4c03288
Ind. Eng. Chem. Res. 2024, 63, 20373−20382

poly(EGMP-*co*-HEMA) = 15 > poly(EGMP-*co*-BUMA) = 3. These calculations demonstrate that both the identity of the spacer molecule and the pH impact the selectivity for UO_2^{2+} over La^{3+}. Thus, incorporating a nonbinding spacer can be a strategy to tune the selectivity for actinyl-lanthanide separations.

3.4.3. Modeling the Membrane Column as a Packed-Bed Reactor. The final step was to assess the feasibility of separating La^{3+} and UO_2^{2+} from the synthesized membrane adsorbers by simulating breakthrough curves. Single species breakthrough curves for 1.1 μM feeds of La^{3+} and UO_2^{2+} were overlaid for comparison. Simulated breakthrough curves for all adsorbers at pH 1 and 4 are shown in Figures S2 and S3. The breakthrough curves for the as synthesized poly(EGMP-*co*-HEMA) and poly(EGMP) membranes at pH 1 are shown below in Figure 7.

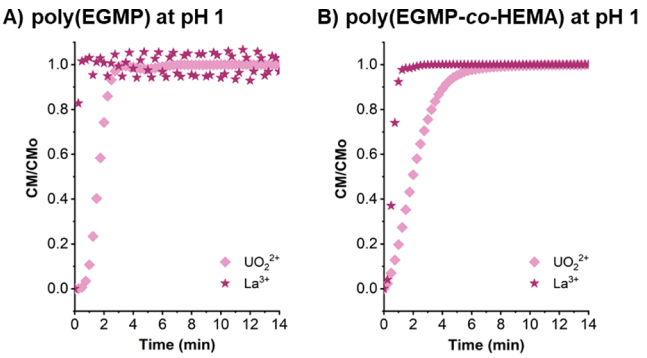

Figure 7. Modeled breakthrough curves for La^{3+} and UO_2^{2+} at pH 1 were obtained using the experimentally determined parameters.

The separation of La^{3+} and UO_2^{2+} can be visualized by the area between the two breakthrough curves, as shown in Figure 7. The larger the area, the greater the separation during the loading step. The separation was quantified by calculating the dynamic binding capacity (μmol adsorbed/g resin) for both species at a process time of 2 min. The ratio of dynamic binding capacities (U/La) describes the separation factor for the two species when loaded on the column. At pH 1 with a flow rate of 1 mL/min, adding HEMA to the poly(EGMP) membrane effectively increases the separation factor of species during loading from 3 to 11 on the column. These calculations support the conclusion that incorporating nonbinding comonomers can tailor the selectivity of actinyl-lanthanide separations in on-column experiments.

4. CONCLUSIONS

In this study, three membranes were functionalized with poly(EGMP), poly(EGMP-*co*-HEMA), or poly(EGMP-*co*-BuMA). Functionalized membranes were evaluated for the uranyl adsorption capacity, affinity, and kinetics at pH 1 and pH 4. The incorporation of noncomplexing copolymers alters the capacity, affinity, and kinetics of the membranes for UO_2^{2+} adsorption. At pH 4, the capacity (Q_m) of poly(EGMP-*co*-BuMA) is half that of poly(EGMP) on a per mmol P basis, while the affinity (K_L) is a factor of 5 higher. At pH 1, the affinity (K_L) of the poly(EGMP-*co*-HEMA)-functionalized membrane is a factor of 3 higher than that of poly(EGMP). Simulated breakthrough curves for single species adsorption experiments indicate the feasibility of separating UO_2^{2+} and La^{3+} from the synthesized materials. Furthermore, the enhanced selectivity predicted by the K_d analysis is observed in the column with an estimated increase of 3 to 11 based on the breakthrough curves. Though the origins of the selectivity are unknown, copolymerizing EGMP with BuMA or HEMA alters the uranyl and lanthanum adsorption on EGMP-coated membrane adsorbers. The impact of the comonomers on the separation factor $\alpha_{U/La}$ for the three membranes is pH dependent. Comonomers at the more acidic pH 1 increase the separation factor; whereas, the comonomers at the less acidic pH 4 decrease the separation factor. Overall, this study demonstrates the feasibility of using nonbinding comonomers to tune the affinity and selectivity of polymer adsorbents.

■ ASSOCIATED CONTENT

Data Availability Statement

Replication Data is available for free online in the Duval Lab Dataverse Collection: "Replication Data for: Membrane adsorbers with copolymer coatings for the separation of actinides from lanthanides (UO_2^{2+} and La^{3+}), Harvard Dataverse, V1.

Supporting Information

The Supporting Information is available free of charge at https://pubs.acs.org/doi/10.1021/acs.iecr.4c03288.

Time-resolved adsorption data for pH 1 and pH 4, fitting parameters for time-resolved adsorption data at pH 1, fitting parameters for time-resolved adsorption data at pH 4, calculated distribution coefficients used to construct Figure 4, values used in the dynamic binding calculations, simulated breakthrough curves for all membranes at pH 1, and simulated breakthrough curves for all membranes at pH 4 (PDF)

■ AUTHOR INFORMATION

Corresponding Author

Christine E. Duval − *Chemical and Biomolecular Engineering, Case Western Reserve University, Cleveland, Ohio 10900, United States;* orcid.org/0000-0002-8630-5483; Phone: 216-368-8613; Email: Christine.Duval@case.edu

Authors

Priyanka Suresh − *Chemical and Biomolecular Engineering, Case Western Reserve University, Cleveland, Ohio 10900, United States;* orcid.org/0000-0002-9512-6161

Lianna Johnson − *Chemical and Biomolecular Engineering, Case Western Reserve University, Cleveland, Ohio 10900, United States;* orcid.org/0000-0002-0396-8426

Complete contact information is available at: https://pubs.acs.org/10.1021/acs.iecr.4c03288

Notes

Portions of this work were previously included in Priyanka Suresh's PhD thesis at Case Western Reserve University, which was deposited in the OhioLINK digital repository: http://orcid.org/0000−0002−9512−6161.

The authors declare no competing financial interest.

■ ACKNOWLEDGMENTS

This work was supported by the National Science Foundation through Grant #2237523 awarded to Case Western Reserve University and the Case School of Engineering at Case Western Reserve University.

REFERENCES

(1) *Imminent Failure of Phosphogypsum Stack in Tampa Bay Exposes Phosphate Industry Risks*. Center for Biological Diversity. https://biologicaldiversity.org/w/news/press-releases/imminent-failure-of-phosphogypsum-stack-in-tampa-bay-exposes-phosphate-industry-risks-2021-04-03/. accessed 2024−August−31.

(2) Veliscek-Carolan, J. Separation of Actinides from Spent Nuclear Fuel: A Review. *J. Hazard. Mater.* **2016**, *318*, 266−281.

(3) Kołodyńska, D.; Hubicki, Z. Investigation of Sorption and Separation of Lanthanides on the Ion Exchangers of Various Types. In *Ion Exchange Technologies*: IntechOpen, Rijeka, 2012. .

(4) Peters, C.; Braekers, D.; Kroupa, J.; Kasyan, O.; Miroshnichenko, S.; Rudzevich, V.; Böhmer, V.; Desreux, J.-F. CMPO-Calix[4]Arenes and the Influence of Structural Modifications on the Eu(III), Am(III), Cm(III) Separation. *Radiochim. Acta* **2008**, *96* (4−5), 203−210.

(5) Vivero-Escoto, J. L.; Carboni, M.; Abney, C. W.; deKrafft, K. E.; Lin, W. Organo-Functionalized Mesoporous Silicas for Efficient Uranium Extraction. *Microporous Mesoporous Mater.* **2013**, *180*, 22−31.

(6) Wei, Y.; Zhang, L.; Shen, L.; Hua, D. Positively Charged Posphonate-Functionalized Mesoporous Silica for Efficient Uranium Sorption from Aqueous Solution. *J. Mol. Liq.* **2016**, *221*, 1231−1236.

(7) Zhu, X.; Alexandratos, S. D. Development of a New Ion-Exchange/Coordinating Phosphate Ligand for the Sorption of U(VI) and Trivalent Ions from Phosphoric Acid Solutions. *Chem. Eng. Sci.* **2015**, *127*, 126−132.

(8) Alexandratos, S. D.; Zhu, X. The Effect of Hydrogen Bonding in Enhancing the Ionic Affinities of Immobilized Monoprotic Phosphate Ligands. *Materials* **2017**, *10* (8), 968.

(9) Alexandratos, S. D.; Zhu, X. Bifunctional Coordinating Polymers: Auxiliary Groups as a Means of Tuning the Ionic Affinity of Immobilized Phosphate Ligands. *Macromolecules* **2005**, *38* (14), 5981−5986.

(10) Alexandratos, S. D.; Zhu, X. High-Affinity Ion-Complexing Polymer-Supported Reagents: Immobilized Phosphate Ligands and Their Affinity for the Uranyl Ion. *React. Funct. Polym.* **2007**, *67* (5), 375−382.

(11) Veliscek-Carolan, J.; Jolliffe, K. A.; Hanley, T. L. Selective Sorption of Actinides by Titania Nanoparticles Covalently Functionalized with Simple Organic Ligands. *ACS Appl. Mater. Interfaces* **2013**, *5* (22), 11984−11994.

(12) Alexandratos, S. D.; Zhu, X.; Florent, M.; Sellin, R. Polymer-Supported Bifunctional Amidoximes for the Sorption of Uranium from Seawater. *Ind. Eng. Chem. Res.* **2016**, *55* (15), 4208−4216.

(13) Chappa, S.; Das, S.; Debnath, A. K.; Sahu, M.; Saxena, M. K.; Pandey, A. K. Spacer Monomer in Polymer Chain Influencing Affinity of Ethylene Glycol Methacrylate Phosphate toward UO_2^{2+} and Pu^{4+} Ions. *Ind. Eng. Chem. Res.* **2016**, *55* (33), 8992−9002.

(14) Kumler, W. D.; Eiler, J. J. The Acid Strength of Mono and Diesters of Phosphoric Acid. The n-Alkyl Esters from Methyl to Butyl, the Esters of Biological Importance, and the Natural Guanidine Phosphoric Acids. *J. Am. Chem. Soc.* **1943**, *65* (12), 2355−2361.

(15) Duval, C. E.; Darge, A. W.; Ruff, C.; DeVol, T. A.; Husson, S. M. Rapid Sample Preparation for Alpha Spectroscopy with Ultrafiltration Membranes. *Anal. Chem.* **2018**, *90* (6), 4144−4149.

(16) Foster, J. C.; DeVol, T. A.; Husson, S. M. Membranes for the Capture and Screening of Waterborne Plutonium Based on a Novel Pu-Extractive Copolymer Additive. *Membranes* **2022**, *12* (1), 3.

(17) Foster, J. C.; DeVol, T. A.; Husson, S. M. Extractive Thin-Film Composite Membranes for the Isotopic Screening of Plutonium in Water. *React. Funct. Polym.* **2021**, *167*, 105020.

(18) Darge, A. W.; DeVol, T. A.; Husson, S. M. Polyamidoxime-Based Membranes for the Rapid Screening of Uranium Isotopes in Water. *Anal. Chim. Acta* **2022**, *1220*, 339997.

(19) Sepesy, M.; Fugate, B.; Duval, C. E. Amine-Functionalized Membrane Adsorbers to Purify Copper from Acidic Solutions. *ACS Appl. Polym. Mater.* **2022**, *4*, 3034.

(20) Suresh, P.; Che, A. C.; Yu, M.; Pataroque, K. E.; Kulbacki, D. K.; Duval, C. E. Incorporating Comonomers into Polymeric Phosphate Ligands Can Tune the Affinity and Capacity for Rare Earth Element, La. *ACS Appl. Polym. Mater.* **2022**, *4* (9), 6710−6722.

(21) Ho, Y. S.; Ng, J. C. Y.; McKay, G. KINETICS OF POLLUTANT SORPTION BY BIOSORBENTS: REVIEW. *Sep. Purif. Methods* **2000**, *29* (2), 189−232.

(22) Qiu, H.; Lv, L.; Pan, B.; Zhang, Q.; Zhang, W.; Zhang, Q. Critical Review in Adsorption Kinetic Models. *J. Zhejiang Univ.-Sci. A* **2009**, *10* (5), 716−724.

(23) Foo, K. Y.; Hameed, B. H. Insights into the Modeling of Adsorption Isotherm Systems. *Chem. Eng. J.* **2010**, *156* (1), 2−10.

(24) Darge, A. W.; Gera, Y.; DeVol, T. A.; Husson, S. M. Uranium Concentration Using Reactive Polymer Thin Films for Spectroscopic Analyses. *React. Funct. Polym.* **2020**, *157*, 104761.

https://doi.org/10.1021/acs.iecr.4c03288
Ind. Eng. Chem. Res. 2024, 63, 20373−20382